Double-sided Polished Ultra-stable and Ultra-sensitive Optical Fiber Sensor

Guowen An[1] · Pinggang Jia[1] · Ting Liang[1] · Yingping Hong[1] · Haiyang Wang[1,2] · Abdul Ghaffar[1] · Jijun Xiong[1]

Abstract

A double-sided polished photonic crystal fiber (DP-PCF) for surface plasmon resonance(SPR) sensing is designed and analyzed by using the finite element analysis software COMSOL 5.5. The suggested design shows strong sensitivity stability in the low refractive index (RI) region (1.33 ∼ 1.39) and ultra-high sensitivity in the high RI region (1.39 ∼ 1.43), respectively. The structural parameters of the proposed sensor are studied to analyze the stability and high sensitivity of the fiber sensor. The introduced DP-PCF sensor offers high sensitivity of 32,434 nm/RIU in the RI range of 1.39 ∼ 1.43 due to its special double-sided polishing design.

Introduction

Surface plasmon resonance (SPR) can occur when a thin metal film is coated on the surface of optical fibers [1]. The energy in the fiber core can be coupled to the surface of the metal layer and form a transmission spectrum trough (signal peak) for sensing. In recent years, more and more scholars have studied and reported on fiber optic sensors based on SPR. Especially with its unique structural advantages, photonic crystal fibers (PCF) are increasingly used in the field of fiber sensing [2]. Some of these sensors are filled with metal inside the fiber to achieve plasmon resonance. Although the sensitivity of this type of sensor is very high, the analytes to be detected still need to be internally filled by special methods. This complicated way of handling can greatly reduce the convenience of the sensor and limits its wide application.

To increase the convenience of SPR-based fiber optic sensors, scholars began to optimize the sensor from the perspective of changing the fiber structural parameters.

Most of the processing methods are to get a smooth platform for metal coating by polishing the side of the optical fiber. As a result, these so-called D-shaped fiber sensors can be inserted directly into the analyte for detection, and the analyte will not have to be filled into the cladding of the fiber by additional means. However, although this method improves convenience, it also brings another disadvantage that can not be ignored; that is, the sensitivity of the sensor is not as high as that of the analyte-filled sensor. For example, in 2015, Luyin et al. proposed a hollow-core PCF filled with silver nanowires, the highest average spectral sensitivity of 14240 nm/RIU was obtained by experiments [3]. Rifat A. A. et al. proposed a multi-core flat fiber SPR-based RI sensor and achieved a maximum sensitivity of 23,000 nm/RIU [4]. There are also many analyte-filled fiber optic sensors whose sensitivity is mostly between 10,000 and 20,000 nm/RIU [5, 6]. However, for D-shaped fibers, the sensitivity is much smaller in comparison (listed in Table 1). From the above examples, it can be found that the sensitivity of the D-shaped fiber sensor is much lower than that of the analyte-filled sensor. It is mainly because the energy coupling surface between the analyte and the fiber core is not large enough. Only one side of the core guided light can be coupled to the metal surface and contact with the analyte.

Those mentioned ideas and disadvantages motivate us to propose a double-sided polished photonic crystal fiber (DP-PCF) sensor, which not only takes into account the convenience but also has relatively high sensitivity. Also, one has found that the sensing mechanism of the DP-PCF

✉ Guowen An
anguowen@nuc.edu.cn

1 Science and Technology on Electronic Test and Measurement Laboratory, North University of China, Taiyuan, 030051, China

2 Department of Physics, University of Ottawa, Ottawa, ON K1N 6N5, Canada

sensor provides ultra-high linearity and stability in the low refractive index (RI) region (1.33 ∼ 1.39) while exhibiting an ultra-high sensitivity comparable to the analyte-filled sensor in the high RI region (1.39 ∼ 1.43).

Structure and Theoretical Modelling

Figure 1 shows the simple yet elegant DP-PCF-based SPR sensor for measuring RI over a wide dynamic range where the sensing area is a section of dual-sided polishing fiber platforms. Chemically stable gold (Au) layers are covered outside the fiber structure to realize a simple detection mechanism. A glass tube with suitable size can be wrapped outside the sensing area to increase the mechanical strength of the sensor. It can be seen in Fig. 1a that the proposed sensor is based on a common polarization-maintaining PCF (PM-PCF). The virtual parts on both sides of the optical fiber represent the polished parts, which are the sensing areas. The large air holes on both sides of the core region responsible for the birefringence effect help to confine the light energy to the central region and are more likely to leak in the Y-axis direction and couple with the metal layer to sense the change of ambient RI.

The section of the SPR sensor has been divided into a large number of homogeneous subspaces, and Maxwell's equations are solved by calculating adjacent subspaces. These subspaces are triangular and can nicely approximate a fiber structure. A perfectly matched layer (PML) boundary condition is considered as a radiation absorber in order to minimize the influence of echo on the calculation results. About fabrication, the selection of general PM-PCFs can reduce the fabrication complexity. The metal film can be obtained according to various methods mentioned in the literature [7–9].

For convenience and maximum sensing sensitivity, all cladding air hole radius is the same to be $r = 1$ μm that can reduce the fabrication complexity. Other relevant structural parameters are as follows: $R = r + 3$ μm, the thickness of metal layer $H = 40$ nm, lattice constant $\Lambda = 6$ μm, the vertical distance of the metal layer from the horizontal plane is $P = \Lambda + 0.2$ μm.

Figure 2 shows the energy transfer relationship between the core mode and SPP mode. Each interval of the figure represents the corresponding energy distribution map at different wavelengths. The small peaks on both sides of the center are the energy peaks corresponding to the metal film coverage areas on the upper and lower sides of the
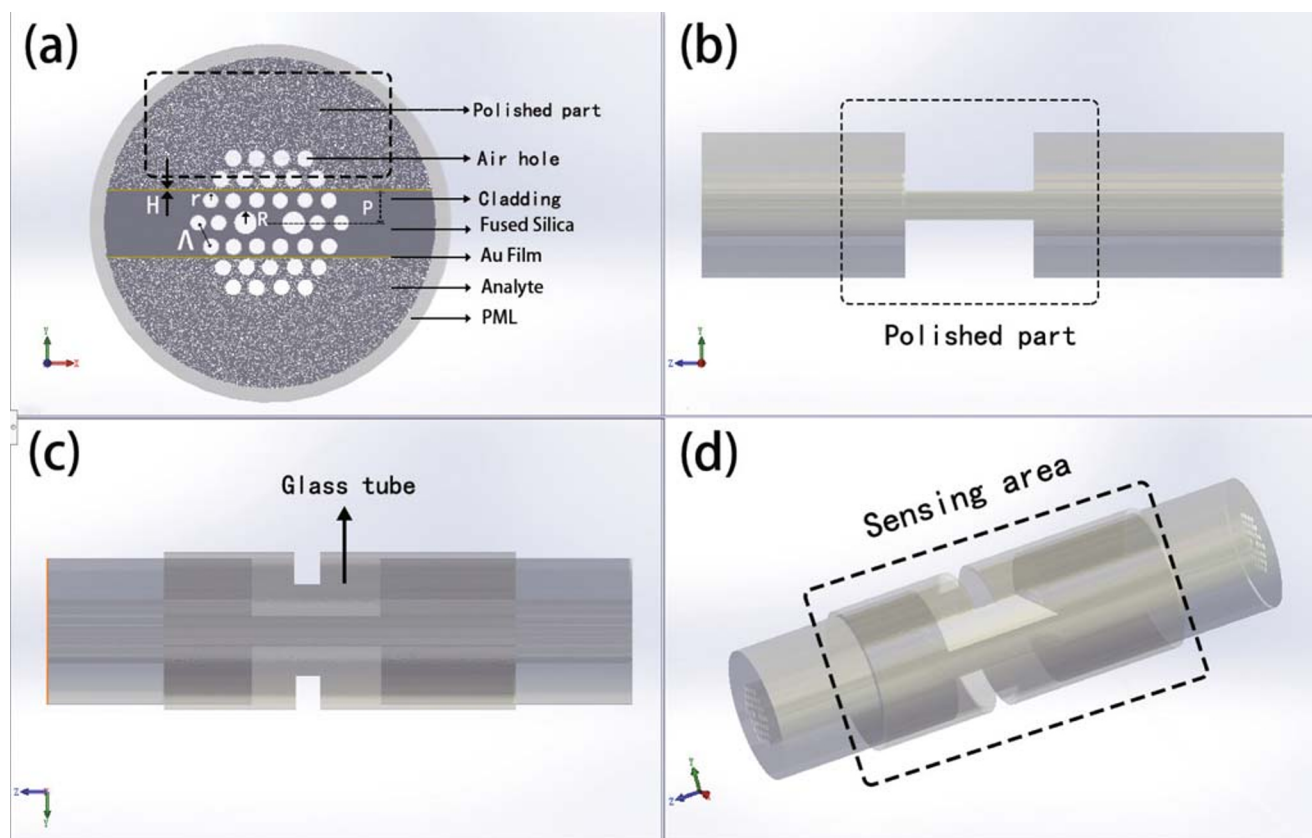
Fig. 1 Cross-sectional view of the proposed structure. **a** Cross-sectional view of the PCF. **b** Double-sided polished PCF. **c** Sensing area of the DP-PCF with glass tube. **d** DP-PCF covered with Au film
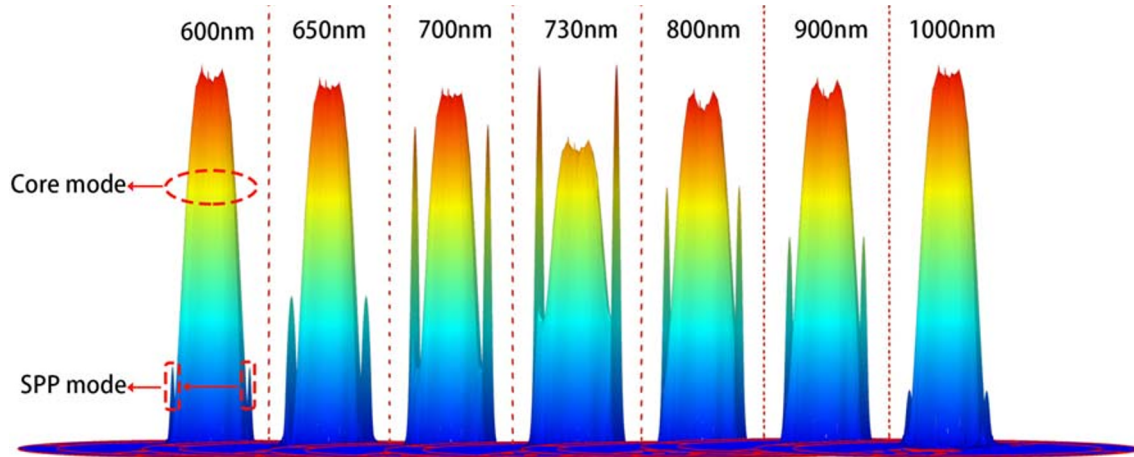
Fig. 2 Schematic diagram of energy transfer when incomplete coupling occurs between core mode and SPP mode

DP-PCF core, that is, the energy of SPP mode. The peak in the center is the energy distribution of the fundamental mode in the core region. When the wavelength is in the short wavelength region of the optimum phase-matching wavelength (< 730 nm), only a small part of the core energy is transferred to the SPP mode. Since the optimum phase-matching point is not achieved, the SPP mode has less energy and a lower peak. As the wavelength increases, more and more core mode energy transfers to SPP mode. It can also be seen from the figure that the energy in the core region decreases, and the energy in the An film-analyte area increases. When the wavelength is matched to the phase-matching point (730 nm), the SPP mode energy reaches the maximum value, and the core region energy has a minimum value. The energy transfer efficiency is the highest. As the wavelength continues to increase toward the long-wave direction (>730 nm), part of the energy transferred from the core mode to the SPP mode is returned to the core region. Throughout the overall coupling process, it can be found that the energy is only partially transformed between the core region and the metal film region, and the mode morphology has never been converted. An incomplete coupling occurs between the core fundamental mode and the SPP mode. Theoretical explanations of the complete coupling and incomplete coupling have been explained in previous work [10], not tired in words here.

Sensitivity and detection accuracy are important indicators to measure the performance of an SPR-based sensor. The aqueous analyte is taken as an example with the dynamic index range from 1.33 to 1.43. We choose the wavelength scanning method as the method of calculating sensitivity, which can be calculated from the equation (1) and achieved by using a broadband light source:

$$S_\lambda(\lambda)(\text{nm/RIU}) = \partial\lambda_{\text{res}}/\partial n_a \tag{1}$$

where λ_{res} refers to the resonance wavelength. For the sake of high performance of the proposed DP-PCF sensor more conveniently and efficiently, we have obtained Fig. 3 in regard to the variation of transmitted spectrum curve and sensitivity within a certain RI range for the sensor mentioned in this article under structural parameters of $\Lambda = 6$ μm, $H = 40$ nm, $P = \Lambda + 0.2$ μm, $r = 1$, $R = r + 3$ μm. As one can see in Fig. 3, with the increase of ambient RI, transmittance spectrum experiences a red shift.

It can be seen from Fig. 4 that the sensing range can be divided into a low RI region and a high RI region according to the fitting precision. The dotted red box on the left side of Fig. 3 represents the low RI sensing region ($1.33 \sim 1.39$) and is hardly affected by parameter changes, which will be discussed later. The linear fitting formula of the low RI region corresponding to the above optimal parameters is
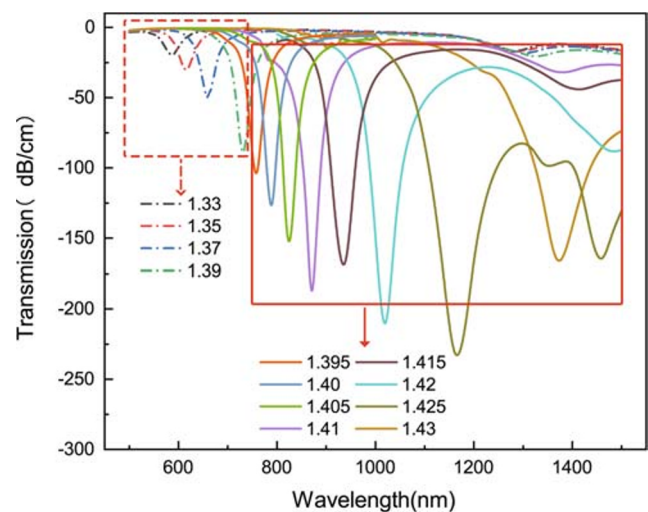
Fig. 3 The transmission spectrum of the sensor varies with the ambient RI
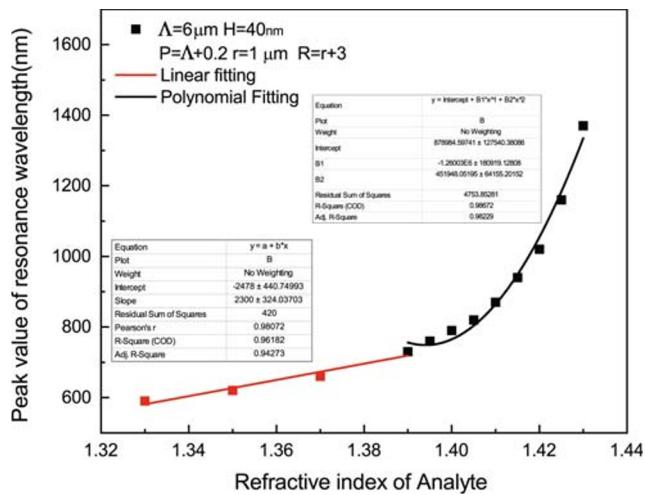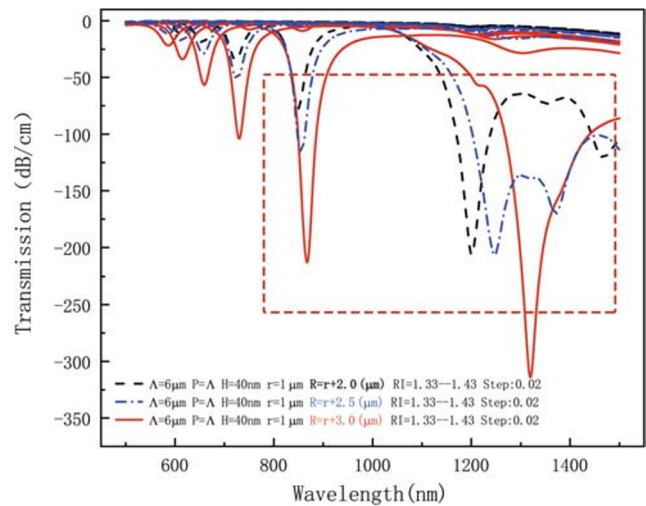
Fig. 4 The sensitivity fitting curve of the sensor varies with the ambient RI

Fig. 5 The effect of the fiber parameter R on the transmission spectrum. (The dotted red box represents the high RI region of 1.39 ~ 1.43)

$y = 2300x - 2478$ with an adjusted R^2 of 0.9618, which represent better goodness of fit. The slope of the fitting formula represents the sensitivity; that is, the corresponding sensitivity is 2300 nm/RIU. The dotted red box on the right side of Fig. 3 represents the high RI sensing region (1.39 ~ 1.43). When the detected RI falls within this range, the sensing sensitivity will be improved, and the optimization of the structural parameters can greatly improve the sensitivity value. It is mainly because, with the increase of ambient RI, the RI difference between the analyte and the optical fiber decreases gradually, and the resonance wavelength also moves to the long-wavelength region. These changes will weaken the ability of the fiber to limit the light field, which is beneficial to the leakage of the light field energy and interact with the analyte, thereby improving the detection capability. Therefore, the quadratic polynomial fitting curve of Fig. 4 shows that the maximum sensitivity at 1.43 is 32,434 nm/RIU. A maximum resolution of 3.08×10^{-6} RIU can be obtained by assuming the spectrometer resolution of $\Delta\lambda = 0.1$ nm.

The sensing performance of related side polished fiber sensors proposed in recent years is listed in Table 1. It can be seen that as fused silica-based optical fibers, its detection range lasted from 1.33 to 1.43. Compared with other sensors

of the same material, it is a relatively wide detection range. For sensitivity, it is very high in the same type of sensors and even more sensitive than most of the analyte-filled PCF sensors.

Result and Discussion

Ultra-high Sensitivity in High Refractive Index Regions

In this section, one focuses on the effects of structural parameter changes on sensing performance in high RI regions, which has been marked by a red dashed box (1.39 ~ 1.43). Figure 5 shows the effect on the sensing performance when the radius (R) of the air holes responsible for the birefringence effect changes. As one can see, with the increase of the radius (R), red shift phenomenon occurs at resonance coupling wavelengths corresponding to different RI ranging from 1.33 to 1.43. Unless otherwise specified, the RI steps between adjacent transmission spectrum troughs are 0.02. When R increases, the resonance wavelength corresponding to the RI = 1.43 is moved from
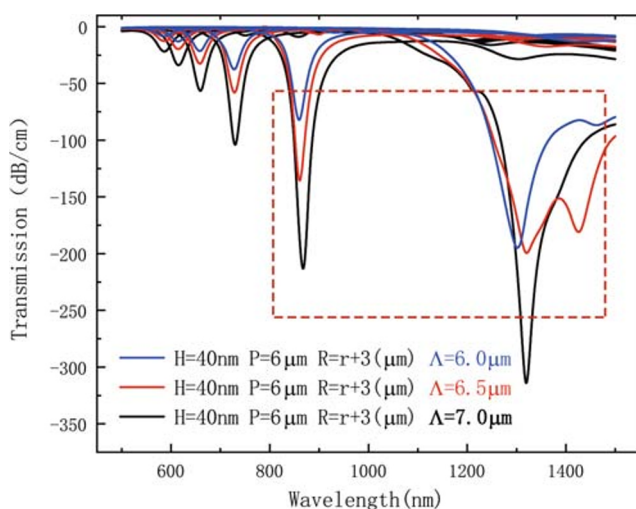
Table 1 Performance comparison table of various side polished optical fiber sensors have been reported

Characteristics	Wavelength (nm)	RI range	Sensitivity (nm/RIU)
Graphene-covered D-shaped fiber [11]	480–650	1.33–1.37	3700 nm/RIU
Dual D-shape [12]	600–1800	1.36–1.41	14,660 nm/RIU
D-shaped, PCF [13]	2300–2900	1.20–1.29	11,055 nm/RIU
D-shaped, PCF [14]	1000–1500	1.43–1.46/	7700 nm/RIU
Graphene with a metal film layer [15]	1650–1750	1.33–1.345	5700 nm/RIU
Double-sided polished (our work)	590–1370	1.33–1.43	32,434 nm/RIU

1200 to 1250 nm. That is to say, in the high RI region, as the radius (R) increases, the corresponding sensitivity also increases. The reason why not to continue to increase the radius (R) is that the larger radius (R) will increase the difficulty of fiber preparation. According to the preparation experience, the fused silica air holes with larger radius are easily collapsed under the graphite furnace's high-temperature environment of $\sim$ 1800 °C. So $R = r + 3$ μm is selected as one of the optimization parameters.

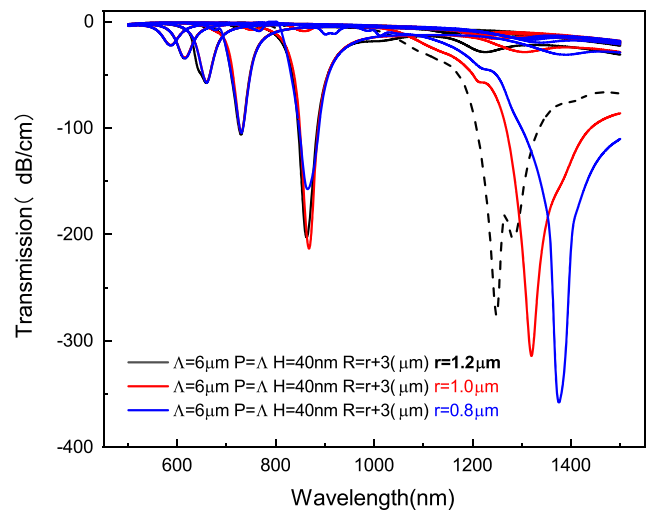Figure 6 shows the influence of lattice constant (Λ) on sensing performance. The coupling strength increases as Λ increases. However, the increase of Λ did not cause much change in sensitivity. That is to say, the small change of lattice constant has little effect on the sensing performance, which greatly reduces the requirement of optical fiber fabrication accuracy.

As one can see in Fig. 7 that with the decrease of r, the transmission spectrum trough corresponding to $n_{(a)} = 1.43$ moves toward the long wavelength. It is mainly because the smaller the radius of the fiber cladding's air hole, the easier the energy of the core leaks out to the outside, thus increasing the sensitivity.

The effect of the change in the height of the metal layer (P) from the center of the core on the sensing performance is shown in Fig. 8. Similarly, the change of the height of the metal layer does not have much effect on the low RI region but influences the sensitivity of the high RI region. With the increase of P, the resonant coupling wavelength in the high RI region shifts to the long wavelength. It can also be found that the core energy coupled to the metal layer becomes less due to the increase of P. Therefore, we choose $P = \Lambda + 0.2$ μm as the optimal parameter which can increase the sensitivity while maintaining a good cross talk (CT).

Fig. 7 The effect of the radius r of the air holes of the cladding on the transmission spectrum. (The dotted red box represents the high RI region of 1.39 ∼ 1.43)

The above discussion is about the influence of the structure parameters of optical fibers on the sensing performance in high RI region. For the SPR-based fiber sensors, the parameters of the covered metal material can seriously affect the coupling efficiency between the core mode and the SPP mode, especially the thickness of the metal layer. With the increase of the thickness (H) of Au layer, as can be seen in Fig. 9a, the resonance coupling wavelengths in the high RI region and the low RI region all experience a red shift; that is, the transmission spectrum troughs move to the long-wave direction. Changes in metal layer thickness will inevitably lead to the change
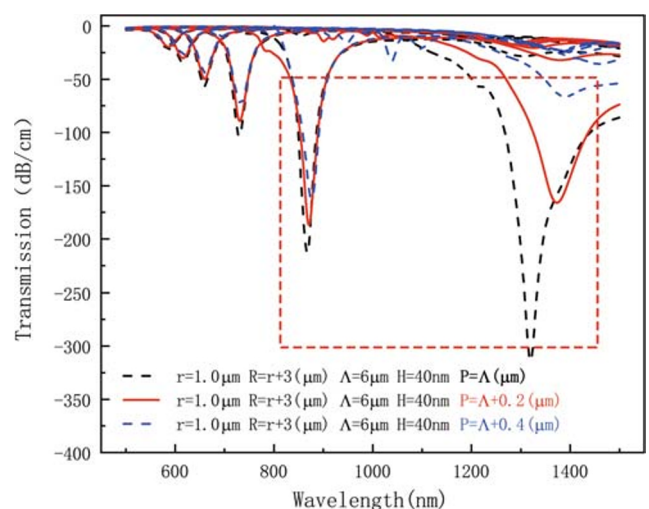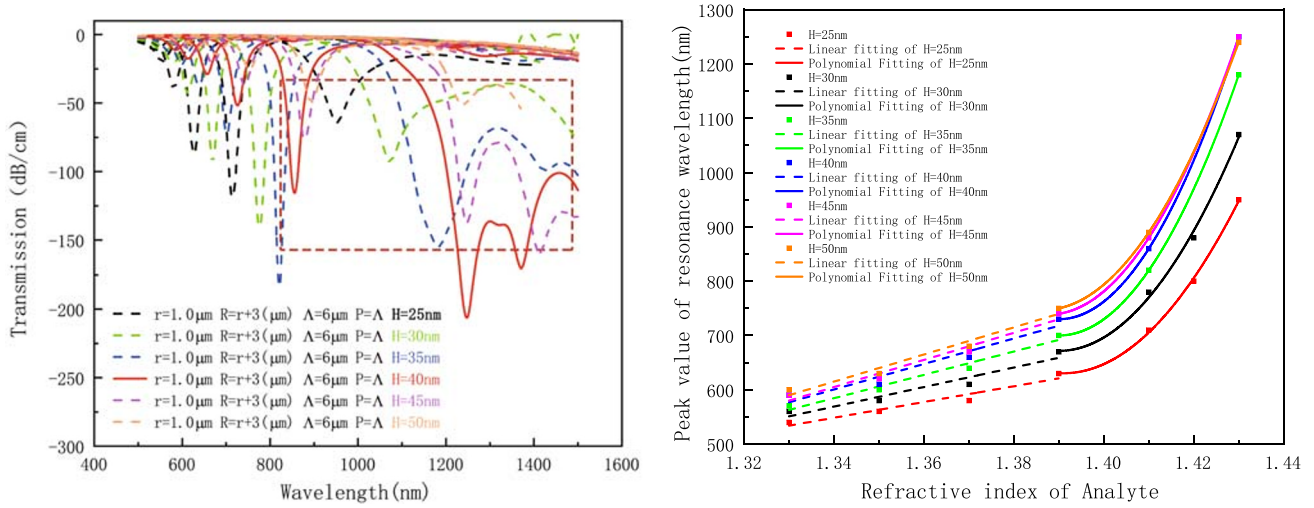

Fig. 6 The effect of the lattice constant Λ on the transmission spectrum. (The dotted red box represents the high RI region of 1.39 ∼ 1.43)

Fig. 8 The effect of the height of the metal layer p on the transmission spectrum. (The dotted red box represents the high RI region of 1.39 ∼ 1.43)

(a) Variation of transmission spectrum with different metal film thickness.

(b) Sensitivity with varying metal film thickness from 25nm to 50nm.

Fig. 9 Effect of metal thickness on the sensing performance

of sensitivity. As can be seen from the figure, when the thickness of the metal layer is 40 nm, the sensitivity is the highest for the high RI region and has a good CT = 106 dB, which determines the influence of unwanted polarization modes [16]. Figure 9 b shows the sensitivity of the fiber varies with the thickness of the metal layer. It can be seen that the thickness of the metal layer still has some influence on the overall sensitivity of the sensor. For the low RI region, the sensitivity increases from 1450 to 2500 nm/RIU as H increase from 25 to 50 nm. For the high RI region, as can be seen, that when H = 40 nm, the slope of the

fitting curve is the largest, which represents the sensitivity of the sensor. Therefore, taking these factors into account, H = 40 nm was selected as the optimum parameter.

Structural Ultra-stability in Low Refractive Index Regions

Not only the sensitivity is an important indicator to measure the performance of a sensor, but its structural stability is another important performance indicator. The stability of the sensor for low RI region is analyzed by combining the
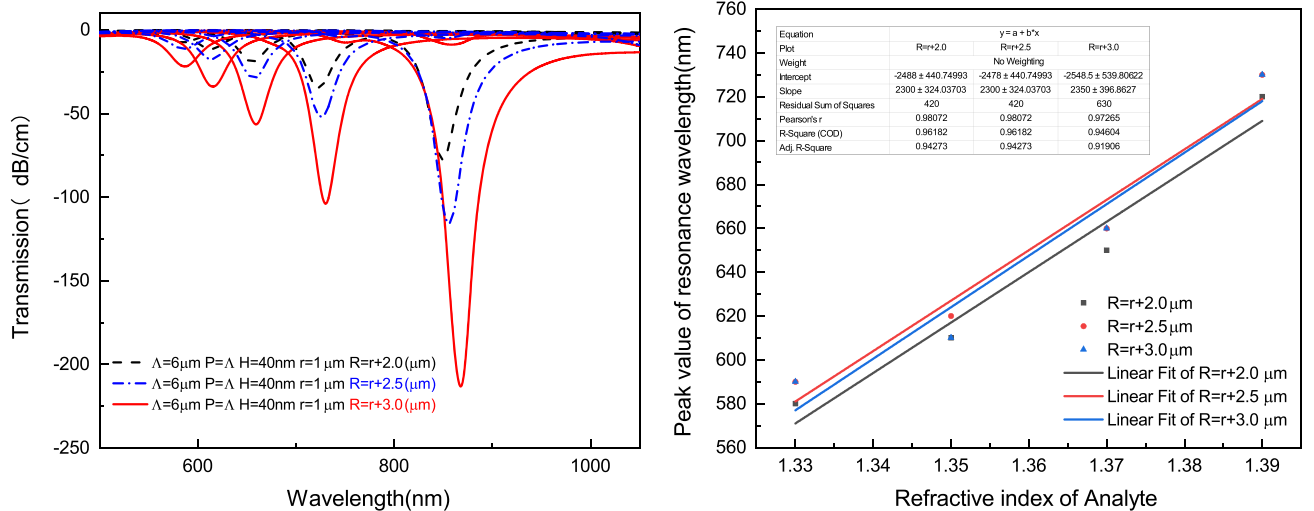
(a) The effect of the fiber parameter R on the transmission spectrum of the low RI region (1.33 ∼ 1.39).

(b) The sensitivity fitting curve of the sensor varies with the parameter R.

Fig. 10 Effect of R on the sensing performance
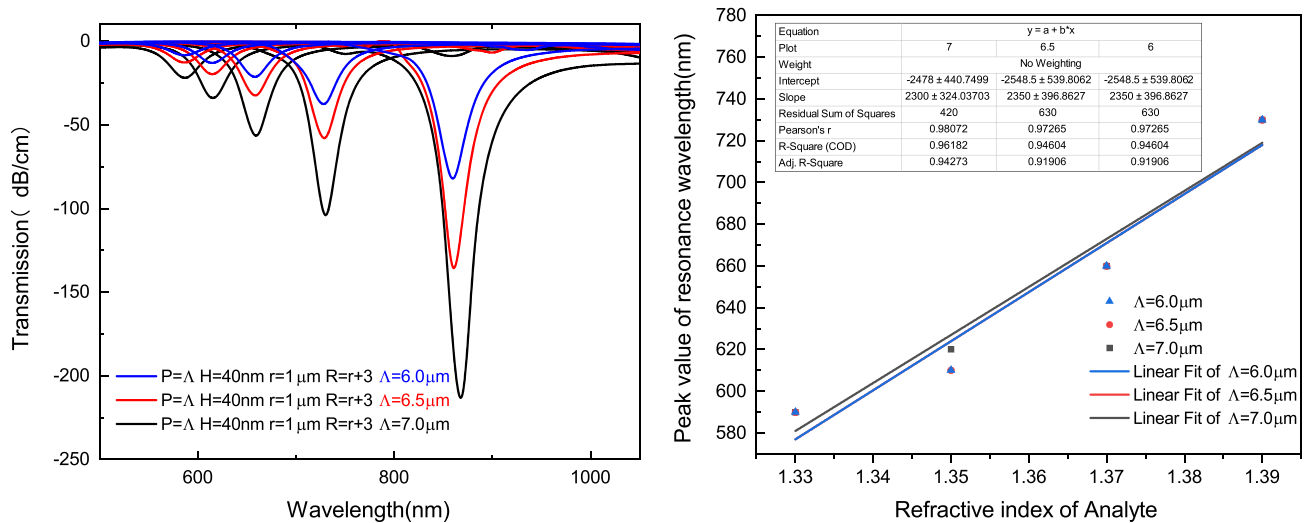
(a) The effect of the fiber parameter Λ on the transmission spectrum of the low RI region (1.33 ∼ 1.39).

(b) The sensitivity fitting curve of the sensor varies with the parameter Λ .

Fig. 11 Effect of Λ on the sensing performance

transmission spectra corresponding to different RI obtained by wavelength scanning method with the linear fitting curve.

As can be seen from Fig. 10a, with the increase of radius R, transmission spectrum troughs corresponding to RI from 1.33 to 1.39 shift slightly toward the long wavelength and the coupling strength between core energy and the metal layer are increased due to the extrusion of the air holes. As can be seen from the linear fitting curve parameters of Fig. 10b, although the radius R is increased by 50%, the sensitivity is only increased by 2%. It can be seen that although the radius of the air holes on both sides of the core

varies greatly, the sensing performance in the RI region does not change much.

Figure 11a shows the effect of changes in the lattice constant of the PCF on the sensing performance. It can be seen that although the lattice constant Λ is increased from 6.0 to 7.0 μm, the sensitivity shown in Fig. 11b is only increased by 2%. The increase of Λ does not cause much drift of transmission spectrum troughs, but only increases the coupling strength.

The influence of the radius of air holes in cladding on the sensing performance is shown in Fig. 12a. The increase of
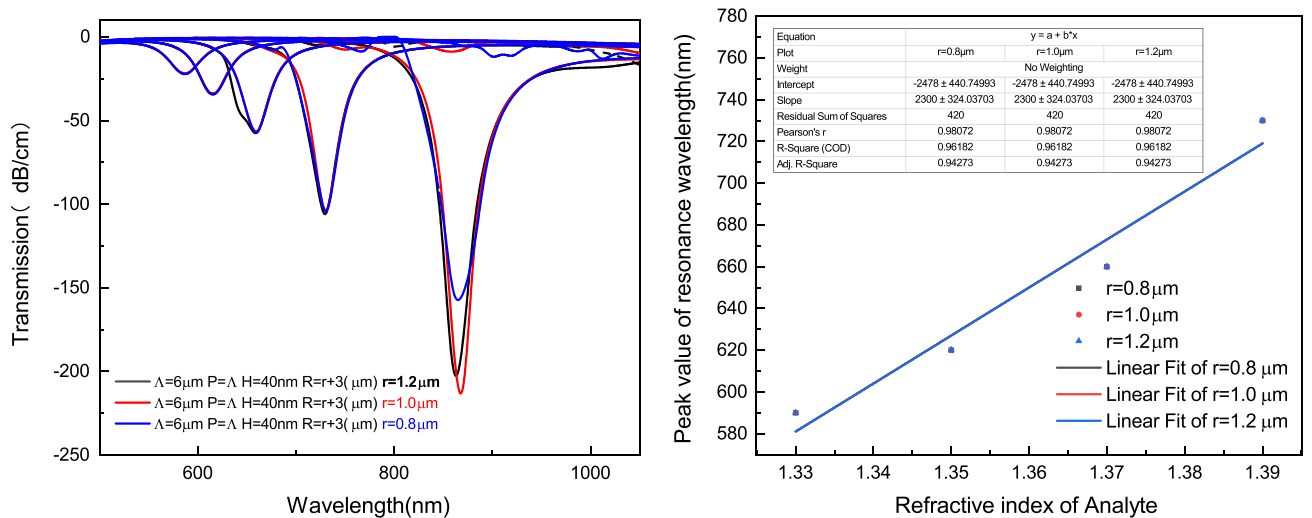
(a) The effect of the fiber parameter r on the transmission spectrum of the low RI region (1.33 ∼ 1.39).

(b) The sensitivity fitting curve of the sensor varies with the parameter r .

Fig. 12 Effect of r on the sensing performance
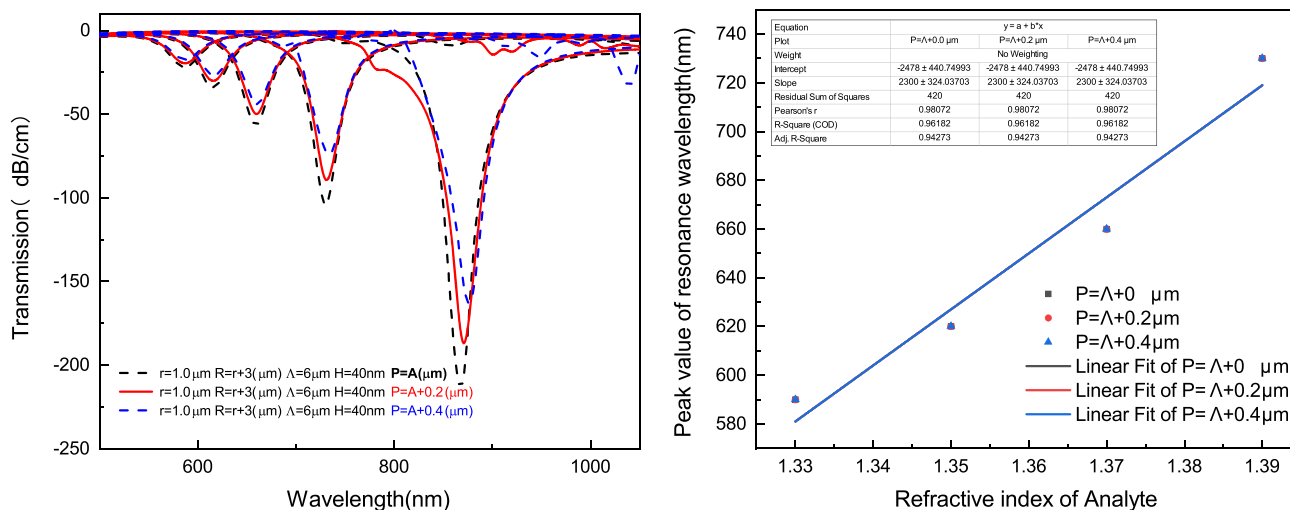
(a) The effect of the fiber parameter P on the transmission spectrum of the low RI region $(1.33 \sim 1.39)$.

(b) The sensitivity fitting curve of the sensor varies with the parameter P.

Fig. 13 Effect of P on the sensing performance

r does not cause any change in sensitivity (Fig. 12b) except for a slight change in coupling strength corresponding to $n_a = 1.39$.

Similarly, as shown in Fig. 13a, changes in the position (P) of the metal layer also cause slight perturbations in the transmission spectrum troughs but do not cause changes in sensor sensitivity (Fig. 13b).

Given the above, for the proposed DP-PCF sensor, small changes in fiber structure parameters will not cause a large change in the sensitivity of the low RI region. In terms of fiber preparation, we can focus more on the coating accuracy of the metal layer, which provides the SPR effects, and select the appropriate fiber structure parameters according to the detection range. Therefore, a precise metal coating process with appropriate structural parameters can ensure a good sensing performance of the proposed sensor and combines the advantages of double-sided polished structure.

Conclusion

The aim of this paper was to describe a proposed RI sensor based on the photonic crystal fiber obtained by the dual-sided polishing method. A simple sensing coupling mechanism is formed by coating Au layers on the polished surfaces. By optimizing the structure parameters, the sensor exhibits ultra-stable sensing characteristics in the low RI region $(1.33 \sim 1.39)$. In the high RI region $(1.39 \sim 1.43)$, due to the concept of double-sided polishing process, its sensitivity is up to 32434 nm/RIU with the corresponding resolution of 3.08×10^{-6} RIU, which is higher than most of the reported sensors of the same type, even can be

comparable to the analyte-filled PCF sensors. The proposed sensor can be an alternative to the previously developed ones.

Compliance with Ethical Standards

Conflict of interests The authors declare that they have no conflict of interest

References

1. Obando LA, Gentleman DJ, Holloway JR, Booksh KS (2004) Manufacture of robust surface plasmon resonance fiber optic based dip-probes. Sensors & Actuators B 100(3):439–449
2. Rifat AA, Mahdiraji GA, Sua YM, Shee YG, Ahmed R, Chow DM, Adikan FRM (2015) Surface plasmon resonance photonic crystal fiber biosensor: a practical sensing approach. IEEE Photon Technol Lett 27(15):1628–1631
3. Lu Y, Yang X, Wang M, Yao J (2015) Surface plasmon resonance sensor based on hollow-core pcfs filled with silver nanowires. Electron Lett 51(21):1675–1677
4. Rifat AA, Mahdiraji GA, Sua YM, Ahmed R, Shee Y, Adikan FM (2016) Highly sensitive multi-core flat fiber surface plasmon resonance refractive index sensor. Opt Express 24(3):2485–2495
5. Li D, Zhang W, Liu H, Hu J, Zhou G (2017) High sensitivity refractive index sensor based on multicoating photonic crystal fiber with surface plasmon resonance at near-infrared wavelength. IEEE Photonics J 9(2):1–8
6. Pathak A, Ghosh S, Gangwar R, Rahman B, Singh V (2019) Metal nanowire assisted hollow core fiber sensor for an efficient

detection of small refractive index change of measurand liquid. Plasmonics, pp 1–8

7. Maruyama T, Fukui K (1991) Indium tin oxide thin films prepared by chemical vapour deposition. Thin Solid Films 203(2):297–302

8. Zheng J, Kwok HS (1993) Low resistivity indium tin oxide films by pulsed laser deposition. Appl Phys lett 63(1):1–3

9. Ali M, Ibrahim K, Hamad OS, Eisa M, Faraj M, Azhari F (2011) Deposited indium tin oxide (ito) thin films by dc-magnetron sputtering on polyethylene terephthalate substrate (pet). Rom J Phys 56(5-6):730–741

10. Zhang Z, Shi Y, Bian B, Lu J (2008) Dependence of leaky mode coupling on loss in photonic crystal fiber with hybrid cladding. Opt Express 16(3):1915–1922

11. Dash JN, Jha R (2015) On the performance of graphene-based d-shaped photonic crystal fibre biosensor using surface plasmon resonance. Plasmonics 10(5):1123–1131

12. Liu C, Su W, Liu Q, Lu X, Wang F, Sun T, Chu PK (2018) Symmetrical dual d-shape photonic crystal fibers for surface plasmon resonance sensing. Opt Express 26(7):9039–9049. https://doi.org/10.1364/OE.26.009039. http://www.opticsexpress.org/abstract.cfmURI=oe-26-7-9039

13. Chen X, Xia L, Li C (2018) Surface plasmon resonance sensor based on a novel d-shaped photonic crystal fiber for low refractive index detection. IEEE Photonics J 10(1):1–9

14. Gangwar RK, Singh VK (2017) Highly sensitive surface plasmon resonance based d-shaped photonic crystal fiber refractive index sensor. Plasmonics 12(5):1367–1372

15. Patnaik A, Senthilnathan K, Jha R (2015) Graphene-based conducting metal oxide coated d-shaped optical fiber spr sensor. IEEE Photon Technol Lett 27(23):2437–2440

16. Hameed MFO, Obayya SSA (2011) Design of passive polarization rotator based on silica photonic crystal fiber, vol 36. shttp://ol.osa.org/abstract.cfm?URI=ol-36-16-3133